Published in final edited form as:
Acad Radiol. 2005 June ; 12(6): 782–792. doi:10.1016/j.acra.2005.01.014.

Preliminary Investigation of Computer-aided Detection of Pulmonary Embolism in Threedimensional Computed Tomography Pulmonary Angiography Images[1]

Chuan Zhou, PhD, **Heang-Ping Chan, PhD**, **Smita Patel, MD**, **Philip N. Cascade, MD**, **Berkman Sahiner, PhD**, **Lubomir M. Hadjiiski, PhD**, and **Ella A. Kazerooni, PhD**
Department of Radiology, University of Michigan, Ann Arbor, CGC B2103, 1500 E. Medical Center Drive, Ann Arbor, MI 48109

Abstract

Rationale and Objectives—We sought to develop a computer-aided diagnosis (CAD) system for assisting radiologists in the detection of pulmonary embolism (PE) on computed tomography pulmonary angiographic (CTPA) images.

Materials and Methods—An adaptive three-dimensional (3D) voxel clustering method was developed based on expectation-maximization (EM) analysis to extract vessels from their surrounding tissues. Using a connected component analysis, the vessel tree was reconstructed by tracking the vessel and its branches in 3D space. The tracked vessels were prescreened for suspicious PE areas using a second EM analysis. A rule-based false-positive (FP) reduction method was designed to detect true PE based on the features of PE and vessels. In this preliminary study, 14 patients with positive CTPA for PE were studied. CT scans were performed at 1.25-mm collimation using a GE LightSpeed CT scanner; eight of these patients also had extensive lung parenchymal or pleural disease. One hundred sixty-three emboli were identified by two experienced thoracic radiologists. The emboli identified by the radiologists were used as the "gold standard." For each embolus, the percent diameter occlusion (clot) and conspicuity of embolus (rating of 1 to 5, with 5 being the most conspicuous) were visually estimated. One hundred one emboli were identified in the six patients without lung diseases; 57 were proximal to the subsegmental and 44 were subsegmental. For the eight patients with lung diseases, 62 emboli were identified, of which 37 were proximal to the subsegmental and 25 were subsegmental. A computer-detected volume was counted as true-positive when it overlapped with an embolus volume identified by the radiologists.

Results—In the cases without lung diseases, if the PE had a conspicuity of >2 and only partially (20%–80%) occluded the vessel, our method detected 92.0% of proximal emboli and 77.8% of subsegmental emboli, with an average of 18.3 FPs/case. In the cases containing extensive lung disease, 66.7% and 40.0% of the PEs were detected with an average of 11.4 FPs/case under the same conditions. For the 14 PE cases, 13 of them were diagnosed as positive PE cases (case sensitivity was 92.9%).

[1]This work was supported by USPHS grant CA093517.

Address correspondence to C.Z. chuan@umich.edu.

Conclusion—This preliminary study indicates that our automated method is a promising approach to CAD of PE on CTPA. Further study is under way to collect a larger data set and to improve the detection accuracy for PE, especially those with <20% or >80% occlusion, and for very subtle PE. A fully developed CAD system is expected to provide a useful aid for PE detection on CTPA.

Keywords

Computer-aided detection; pulmonary embolism; vessel tracking; image segmentation

Pulmonary embolism (PE) is a common, potentially fatal condition associated with significant morbidity and mortality in untreated patients. Prompt and accurate diagnosis of PE greatly influences patient outcome (1-3). Unfortunately, the clinical diagnosis of PE is unreliable and difficult, because symptoms are often vague and nonspecific, leading to misdiagnosis. Computed tomographic pulmonary angiography (CTPA) is an effective means for clinical diagnosis of PE (4-11). CT has advantages over V/Q scan because of its direct imaging of the blood clot, better interobserver agreement, greater accuracy, and possibility to explain patient's sign and symptoms. Previous studies (4,12-24) have shown the specificity of CT to range from 78% to 100% for detection of PE, with large variations in sensitivity from 53% to 100%. For interpretation, the CTPA images must be reviewed on a workstation using a cine-paging mode, with the reader scrolling in and out of individual arteries. The signs of PE include a central intravascular filling defect outlined by contrast material within the vessel lumen, eccentric tracking of contrast material around a filling defect, and complete vascular occlusion. However, each CT scan for PE produces an average of about 300 axial images with a range of 200–600. Multiplanar reconstruction viewing of vessels further increases the number of images to be read. Interpretation of a CT study demands extensive reading time from a radiologist who has to visually track each vessel, distinguish arteries from veins and bronchi, adjust window and level settings, and inspect each artery for possible PE on a workstation. If no obvious PE is found in a suspected PE case, radiologists have to diligently check all arteries before PE can be ruled out. If a positive PE diagnosis is made, although radiologists do not need to identify every PE location in a case, the extent and anatomic location of all PEs should be documented for prognostic purpose and follow-up examination. The advent of multidetector CT offers the possibility of detecting subtle PE in subsegmental arteries, but it also makes CTPA interpretation an even more demanding task. It is difficult to review small subsegmental vessels, not only because of the large number of these vessels but also because of their lower conspicuity due to partial volume effects. False-negatives (FNs, missed diagnosis) may occur due to the complexity of the images and the large number of vessels to be tracked in each case.

Computer-aided diagnosis (CAD) may assist radiologists in PE detection by reducing the chance of missing PE. Using a computer to automatically detect PE on CT images is a new and challenging task. The methods developed so far are very preliminary. Masutani et al (25) developed a computerized method for PE detection based on volumetric image analysis. After segmentation of pulmonary vessels to limit the search space, feature analysis for detection of thrombi was performed inside the segmented vessel volume; 19 (11 positive and 8 normal) cases were selected from 30 clinical cases for performance evaluation. The cases with strong motion artifacts, unsatisfactory opacification, or other diseases that would make computerized detection difficult were excluded from their database. One radiologist marked 21 thrombi in the 11 positive cases. Their results indicated that, when the PE volume was between 16 mm^3 and 64 mm^3, sensitivity was 100% and 85% with 7.7 and 2.6 false-positives (FPs) per case, respectively. Among the 143 FPs for all cases, 92% were related to soft tissues, such as lymphoid tissue surrounding vessels. The results obtained in this study are reasonably good. However, the number of true thrombi in the data set was small, and patients with other diseases were excluded. Furthermore, the report did not describe the characteristics of the true thrombi, such as size, the anatomic distribution and the size distribution of the vessels where PE was

found, and the percentage vessel occlusion by PE, which would reveal the degree of subtlety of the PEs in the study. Schoepf et al (26) recently presented a study of computerized PE detection on CT. They obtained a sensitivity of 91% and 66%, respectively, for 130 segmental emboli and 150 subsegmental emboli in 15 cases, where the "gold standard" for true emboli was determined by two radiologists. Although they used a relatively large number of samples of emboli in their study and achieved a reasonable sensitivity, they did not mention how many FPs were found at these sensitivities. Again, no analysis of the characteristics of the true emboli was given, except for the numbers of emboli in segmental and subsegmental arteries. These preliminary studies indicate that computerized PE detection is at an early stage of development, and much more effort is required to bring this CAD application to clinical practice.

We are developing computer vision techniques for the automatic detection of PE on CTPA images (27,28). In this preliminary study, we designed a prototype system using a small data set to demonstrate the feasibility of our approach. We also analyzed some of the PE characteristics that may impact the detection performance of the system.

MATERIALS AND METHODS

Materials

Fourteen CTPA studies from 14 patients at the University of Michigan were collected with the approval of our institutional review board (IRB). The cases were collected retrospectively without identification. Informed consent was waived by the IRB. The images were acquired with four-slice GE LightSpeed CT scanner at 120 kVp, 380–440 mAs, and reconstructed at 1.25-mm slice thickness. Of the 14, 8 had extensive lung parenchymal or pleural disease.

All cases were diagnosed as positive PE cases during the patients' clinical care. Two experienced thoracic radiologists identified the PE locations, which were used as the "gold standard" for algorithm development and evaluation. The radiologists visually inspected the CTPA images displayed on a monitor with a graphical user interface. The graphical user interface has functions allowing radiologist to cine-page through the CT slices, scroll in and out of individual arteries, adjust window setting, and zoom to improve visualization. Readers marked the PE in every artery on every image they were present. For a single volume of PE that occluded more than one level of the arteries, as well as branches of arteries at the same level, the radiologists virtually split the single PE volume into volumes according to the branching of the artery by marking the PE segment in each branch as a separate PE. For each PE, radiologists marked the approximate location of its center and the starting and ending slices of the PE segment with a cursor, identified the anatomical level of the artery (pulmonary trunk, main, lobar, segmental, and subsegmental), measured the diameter of the vessel with an electronic ruler, visually estimated the percentage of PE occlusion in the artery, and provided a conspicuity rating on a scale of 1 to 5 (5 is the most conspicuous). The conspicuity of the PE indicates the degree of subtlety of the PE in the CTPA images as perceived by experienced radiologists. Although the latter two estimates by the radiologists were very subjective, they would provide some information on how the computer performance was related to the degree of difficulty of the PEs.

The two radiologists identified 163 PEs in the 14 CTPA cases; 69 and 94 of them were located at the subsegmental artery level and the arteries proximal to the subsegmental, respectively. The arteries proximal to the subsegmental level included the pulmonary trunk, main, lobar, and segmental arteries and were referred to as "proximal" arteries in this study. One hundred one PEs were identified in the six cases without lung diseases; of which 44 and 57 were located in the subsegmental and the proximal arteries, respectively. For the eight cases containing extensive lung diseases, 62 PEs were identified, of which 25 and 37 PEs were located at subsegmental and proximal arteries, respectively. The "gold standard" PEs occupied CT slices

ranging from 1 to 75 slices, and the occlusions of arteries by PEs were estimated to be in the range of 5%–100% by radiologists visually.

Vessel Segmentation

Because PEs occur only inside pulmonary vessels, segmentation and tracking of vessels constitute the fundamental steps to limit the search space for identifying ROIs that contain suspicious PEs. Many of the published vessel segmentation and tracking methods provided accurate results in two- or three-dimensional (2D or 3D) images. However, few studies have been conducted for segmentation, tracking, and reconstruction of the pulmonary vessel tree on CTPA images because the pulmonary vessels are more complicated compared with the vessels in other parts of the body in several aspects: widely distributed CT values, large variations of vessel sizes ranging from 1 to 20 mm, and the complicated branching structures. For the PE diagnosis task, it is difficult to track or segment vessel structures in 3D volume using global thresholding or region growing methods (6,29), which are often used in segmentation and visualization of vessels, because pulmonary vessels cannot be accurately segmented and continuously tracked if they are largely or totally obstructed by PE.

As shown in Figure 1, the voxel value histogram of a typical CTPA image exhibits several peaks that generally correspond to the lung region (P1), the chest wall (P2), the soft tissue region (P3), and vessels (P4). To separate these regions, a multistage adaptive 3D segmentation method was developed to cluster voxels into body part, chest wall, lung region, and vascular structures based on Expectation-Maximization (EM) analysis. The vascular structure segmentation was further refined by applying EM-based 3D segmentation algorithm in a local region.

EM was proposed as an algorithm to be used for estimation of missing model parameters (30). It can also be defined as a probabilistic counterpart to fuzzy clustering. Image segmentation can be reformulated as a “missing data” problem if we assume that each image pixel is produced by a probability density associated with one of the segments. To produce an image pixel, a segment is first selected and then the pixel is generated from the density associated with the segment, as

$$p(x)=\sum_i p(x|\theta_i)\pi_i, \tag{1}$$

where π_i is the *prior* for the *i*th segment and represents a set of parameters for the density function associated with the *i*th segment. For the segmentation task, given a set of image pixels, the inverse problem needs to estimate the parameters and the labels for all the pixels. The EM iteration can be used for estimation of these parameters. The labels for all the pixels can be estimated by the method of *maximum a posterior* (MAP), given the estimated density parameter by the EM algorithm.

In our study, we assumed that the number of components (or segments or classes) is known. The same number of Gaussians with equal variances was placed equally across the histogram of the image as the initial estimates. After several iterations, the EM segmentation algorithm found the optimally fitted Gaussians to the histogram. It output the segmented image components when convergence was reached.

Figure 2 shows the automated vessel segmentation scheme using the EM algorithm. The lung region, chest wall, and thoracic vascular structures including the pulmonary arteries and surrounding soft tissues were sequentially segmented based on their relative CT values as shown in the example of a histogram in Figure 1. The vessel segmentation was performed in

three steps. In the first step, the volume containing several slices centered at the current slice was read from the case file and the histogram was generated for the CT values within this volume. The air region outside the patient body was separated by thresholding with a fixed threshold CT value V_1. The EM segmentation was applied to the histogram above V_1 to classify the voxels into two classes: class 1 was the lung region represented by peak P_1 in Figure 1b, and class 2 included the chest wall, soft tissues, and the thoracic vascular structures. In the second step, the same procedure was applied to the class 2 region of the histogram. Again the EM segmentation was used to classify the voxels as the chest wall, soft tissues, and thoracic vascular structures. In this step, some, or occasionally all, of the soft tissues could be misclassified as chest wall or as vascular structures, depending on the CT values of soft tissues in the sequential slices. In the third step, the histogram of voxels classified as the vascular structures was generated. The vessels were finally extracted from their surrounding background including soft tissues and air region inside the lung region by a third EM segmentation. Figure 3 shows an example of the sequential vessel segmentation results.

Vessel Tracking

At the third EM segmentation step, vessels were segmented from their surrounding tissues. The connectivity of the segmented vessels in different slices was determined by a "connected component analysis," in which the vessels were tracked and reconstructed in 3D space as follows.

The iterative procedure for vessel tracking began from a given initial seed point and was applied repeatedly in the local segmented vessel area from the initial slices. The seed point of a vessel to be tracked was chosen interactively by the operator in this pilot study. A connected component analysis was applied to each segmented vessel area in the current slice. Whether the segmented vessel areas in the previous and the next slices were connected to the current slice was determined based on 26-connectivity. The connected vessel areas were stored in a queue as possible branches of the vessel tree. The branches were subsequently tracked after tracking of the main vessel was completed. The above procedure was repeated until the queue was empty. Figure 4 shows an example of a tracked vessel tree. Features extracted from the skeleton and the volume of the segmented regions were used to prevent the vessel from being tracked into the chest wall, the heart area, and other nonvessel areas.

Pulmonary Embolism Detection

The diagnosis of PE on CTPA is based on finding filling defects within the contrast-enhanced lumen of the pulmonary arteries. Defects may partially or completely fill the arteries and have lower CT values compared with CT values in the normal arteries. Partial filling defects often manifest as an area with lower CT values located in an intravascular region surrounded by a variable amount of contrast material that exhibits higher CT values. The partial filling defect can also be manifested as an area with lower CT values located at the marginal region of the vessel. Complete filling defects refer to the area where the entire arterial cross section has low attenuation or low CT values.

After segmentation and tracking of the pulmonary vessels, feature analysis for the detection of PE was performed in the areas around the segmented vessels. The PEs were detected in two steps: prescreening to extract regions containing suspicious PEs, and FP reduction to determine true PEs.

In the prescreening step, a new EM segmentation was applied to the local volume of the segmented vessel. The local volume was constituted from several slices (five slices in this study) of vessel segments that were determined to be a connected vessel in the previous step. Because the segmentation of the vessel in the previous stage was not very accurate, it could

contain lung area background, soft tissues and/or PE, and regions of the vessel. For the EM segmentation, therefore, the number of classes was assumed to be three. In the local volume, if there was no soft tissue surrounding the vessel region and no PE, two of the Gaussian distributions on the histogram could overlap and merge. The final segmentation in this case would include only two classes: the lung area background and the vessels. If there was soft tissue surrounding the vessel and/or PE in the local volume, the final segmentation would contain three classes: lung area background, soft tissue and/or PE, and vessels. Because the CT values of PEs are very close to those of soft tissue, PE and soft tissue would be segmented into the same class. If the EM segmentation resulted in three significant Gaussians, then this local volume would be assumed to contain suspected PE and subjected to the FP reduction at the next step.

The second step in our preliminary PE detection method was FP reduction. In this study, a rule-based classifier was trained to identify true PEs using features extracted from the 2D slices and the 3D volume. The major features used in the classifier included the CT values, edge gradient, and morphological features. The CT value was used to identify PE regions of which the CT values were generally lower than those of the contrast-opacified region of vessels. The edge gradient criterion was used to identify the boundary between PE and the surrounding structures. The morphological features included the shape of the segmented volume in comparison to the local vessel characteristics such as roundness and compactness, and the volume of the PE candidate. In this study, a threshold of two slices was set to be the minimum length of a true PE.

RESULTS

Table 1 shows the results of computerized PE detection when the conspicuity of PE was greater than 2 and the PE only partially (20%–80%) occluded an artery. The computer-detected VOI was counted as true-positive (TP) when it was overlapped with 10% or more of the PE volume identified by the radiologists. For the six PE cases without lung diseases, our method detected 92.0% and 77.8% of the PEs in the proximal and subsegmental arteries, respectively, with an average of 18.3 FPs/case. For the eight cases containing extensive lung disease, 66.7% and 40.0% of the PEs could be detected with an average of 11.4 FPs/case under the same conditions. If the PEs that occurred in the subsegmental and the proximal arteries were considered together, the sensitivity of PE detection was 88.2% and 58.8% for the cases without and with lung disease, respectively. For all 14 cases, the sensitivity was 83.8%, 64.3%, and 78.4% for PEs in the proximal, subsegmental, and all arteries together, respectively.

Table 2 shows the computer performance when the PE occluded a vessel ≤20% or ≥80% and the PE conspicuity was greater than 2. The result indicated that over 60% (63.6% and 66.7% for the cases with and without extensive lung diseases, respectively) of the PEs in proximal arteries could be detected, and more than 30% (33.3% for both the cases with and without extensive lung diseases) of the PEs in subsegmental arteries could be detected if the percentage of the PE occlusion was less than 20%. For the PE occluding more than 80% of a vessel, in the cases without lung disease, 73.3% and 37.5% of the PEs in the proximal and subsegmental arteries could be detected. However, the sensitivities were lower for the cases containing extensive lung diseases (41.7% and 14.3% in proximal and subsegmental arteries, respectively).

Table 3 summarizes the performance of the computer algorithm for all the 163 “gold standard” PEs, regardless of conspicuity ratings, identified in artery branches with occlusion in the range of ≤20%, 20%–80%, and ≥80%. In the six cases without other lung diseases, our method could detect 75.4% (43 of 57) and 38.6% (17 of 44) of the PEs in the proximal and subsegmental arteries, respectively. In the eight cases with extensive lung diseases, 54.1% (20 of 37) and

20.0% (5 of 25) of the PEs could be detected in the proximal and subsegmental arteries, respectively

For the 14 positive PE cases, 92.9% (13 of 14) of them were found to be containing PE positively. The one case that failed to be detected as positive contained only one PE clot located in a subsegmental artery with a radius less than 2 mm and with 90% PE occlusion.

Figure 5 shows examples of detection results. Figures 5a, 5c, and 5e are original images. The black contour in Figure 5b marks a TP PE (40% occlusion and conspicuous is 5) detected in the right posterior lobar artery, and that in Figure 5d marks another TP PE (30% occlusion and conspicuous is 3) detected in the right upper segmental artery. Two examples of FP PEs are shown by white contours in Figures 5b and 5f. The one shown in Figure 5b was a lymphoid tissue surrounding the main artery detected mistakenly as PE, and the other one shown in Figure 5f was due to partial volume effect in the lateral basal subsegmental artery.

DISCUSSION

We are developing a CAD system for detection of PE in 3D CTPA data sets. Computerized PE detection is a challenging task, not only because of the large volume of data but also because of the complexity of the images and the partial volume effect, motion, or other imaging conditions. Our computerized PE detection method was based on vessel segmentation and tracking. Segmentation of vessels occluded by PEs is difficult, especially when the PEs appeared to be connected to the vessel wall and the soft tissues surrounding the vessels. It is also difficult to segment the vessels in regions affected by other lung diseases. Figure 6 shows some examples of these difficult cases. In our pilot study, a small data set was selected from the in-patient files. About half of these cases (8 of 14) contained extensive lung diseases such as parenchymal or pleural disease, which increased the difficulty for the tasks of vessel segmentation, tracking, and PE detection.

In this feasibility study, we found that our current methods are effective in detecting PE that partially occludes an artery (PE occlusion between 20% and 80%) but is less effective for PE with very small (≤20%) or very large (≥80%) occlusion. Our method for prescreening PE locations was based on the assumption that there were three classes of gray level structures (lung area background, soft tissue or PE, and vessels) in the VOI containing the tracked vessel. The EM algorithm was used to detect the peak in the gray level histogram of the VOI corresponding to the voxels of the PE and soft tissue. If the PE was small (occlusion ≤20%) so that the VOI contained small percentage of PE, the peak corresponding to the PE in the histogram would be small and appeared to merge with its adjacent big peak. The FP rate of small PE was therefore relatively high (Table 2). On the other hand, if an artery was occluded by a PE for more than 80%, the small peak corresponding to the small percentage of the contrast-filled artery (higher intensity) could merge with its adjacent large peak on the gray level histogram. The “three classes” again would become two classes (lung area background and soft tissue/PE). If the CT values of the soft tissue/PE peak were lower than a predefined threshold, then it was assumed to be a PE candidate and was sent to the next step for FP reduction. Therefore, some of the PE with large percentage occlusion could still be detected as shown in Table 2.

Table 3 shows the computer performance for PE detection at any conspicuity levels (1-5) for PE occlusion of ≤20%, in the range of 20%–80%, and ≥80%. In this table the PE conspicuity was not used to rule out the PEs that were considered visually difficult as presented in Tables 1 and 2. Comparing the results in these tables, for PEs occlusion between 20% and 80%, the decreases in the sensitivity were about 3.6% and 5.1%, respectively, for PEs located at the proximal and subsegmental arteries for the cases without other lung diseases. For the cases

containing extensive lung diseases, the decreases in the sensitivity were 9.6% and 6.7%, respectively, for PEs located at the proximal and subsegmental arteries. For PEs occlusion of ≤20% and ≥80%, the decreases in sensitivity ranged from 4.5% to 9.5% for the cases without other lung diseases. For the cases containing extensive lung diseases, the sensitivity did not change whether the PEs were located at the proximal or subsegmental artery if the PE occluded an artery ≥80%. However, the number of PEs in these subsets was small so that the uncertainties would be large. The dependence of the computer performance on the conspicuity and percentage occlusion of the PEs need to be further investigated when a large data set is available for analysis in the future.

In clinical practice, a CTPA study is determined to be positive once a PE is identified. However, it is not possible to call an examination negative for PE unless all of the arteries, especially the small subsegmental ones, have been evaluated. Although the clinical significance of small emboli has not been established, small emboli may produce significant morbidity in patients with underlying cardiopulmonary disease (11). In addition, small emboli may indicate a risk for recurrence of more significant emboli. In order for a CAD system to be useful for PE detection, it is important that the CAD system can identify small emboli, which may be more easily be overlooked by radiologists if they are the only PE in a case. The detection sensitivity of a CAD algorithm for individual PEs in a case can be treated, in a way, as the collective evaluation of the sensitivity of PEs of different degrees of occlusion and conspicuity that may occur in many PE cases. Therefore, in the developmental process of a CAD system, it is useful to evaluate the sensitivity for detection of individual PEs as well as the case as a whole. The preliminary results indicate that our current algorithm has relatively high sensitivity for PEs in the proximal arteries, especially in patients without extensive lung diseases. Our results also reveal the difficulty of detecting PE in arteries with less than 20% occlusion or greater than 80% occlusion, PE in subsegmental arteries, and PE in patients with extensive lung diseases. Further development of our computerized method is needed to improve its sensitivity and reduce FP detection.

The performance of a CAD algorithm depends strongly on the degree of difficulty of the lesions to be detected in the data set. In this study, we analyzed the detection performance of our prototype system on subsets of PEs based on their conspicuity, percentage of vessel occlusion, the anatomical level of the vessel where the PE occurred, and the presence of other lung diseases. The analysis is important for the understanding of the weaknesses of the current system so that new techniques targeting these areas can be designed in future development, as well as for comparison with other CAD systems in the future. A major limitation of our analysis is that the sample size is small. On the other hand, although the specific values will contain large uncertainties, the results should reveal the general trend of the dependence of the algorithm performance on these factors. We will continue to expand our database and to improve the analysis in future investigations.

CONCLUSION

Our preliminary study indicates the feasibility of automated tracking of pulmonary arteries and identification of PEs on CTPA images using computer vision techniques and the potential of developing a CAD system for PE detection. Investigations are under way to further improve the performance and evaluate the CAD system with a large data set. When the methods are fully developed, the CAD system is expected to provide an efficient and effective screening method for PE detection on CT scans and to alert radiologists to locations with suspected PEs.

References

1. Dalen J, Alpert J. Natural history of pulmonary embolism. Progr Cardiovasc Dis 1975;17:257–270.

2. Investigators P. Value of the ventilation/perfusion scan in acute pulmonary embolism. Results of the Prospective Investigation of Pulmonary Embolism Diagnosis (PIOPED). JAMA 1990;263:2753–2759. [PubMed: 2332918]

3. Price D. Pulmonary embolism. Prophylaxis diagnosis and treatment. Anaesthesia 1976;31:925–932. [PubMed: 970590]

4. Remy-Jardin M, Remy J, Wattinne L, Giraud F. Central pulmonary thromboembolism: diagnosis with spiral volumetric CT with the single-breath-hold technique-comparison with pulmonary angiography. Radiology 1992;185:381–387. [PubMed: 1410342]

5. McCollough C, Zink F. Performance evaluation of a multi-slice CT system. Med Phys 1999;26:2223–2230. [PubMed: 10587202]

6. Rubin GD, Paik DS, Johnston PC, Napel S. Measurements of the aorta and its branches with helical CT. Radiology 1998;206:823–829. [PubMed: 9494508]

7. Stein P. Reassessment of pulmonary angiography for the diagnosis of pulmonary embolism: Relation of interpreter agreement to the order of the involved pulmonary arterial branch. Radiology 1999;210:689–691. [PubMed: 10207468]

8. Ghaye B. Peripheral pulmonary arteries: How far in the lung does multidetector row spiral CT allow analysis? Radiology 2001;219:629–636. [PubMed: 11376246]

9. Raptopoulos V, Boiselle P. Multi-detector row spiral CT pulmonary angiography: comparison with single-detector row spiral CT. Radiology 2001;221:606–613. [PubMed: 11719653]

10. Schoepf U. Subsegmental pulmonary emboli: improved detection with thin-collimation multi-detector row spiral CT. Radiology 2002;222:482–490.

11. Diffin D, Leyendecker J, Johnson S, et al. Effect of anatomic distribution of pulmonary emboli on interobserver agreement in the interpretation of pulmonary angiography. AJR Am J Roentgenol 1998;171:1085–1089. [PubMed: 9763002]

12. Mayo J, Remy-Jardin M, Muller N. Pulmonary embolism: Prospective comparison of spiral CT with ventilation perfusion scintigraphy. Radiology 1997;205:447–452. [PubMed: 9356627]

13. Qanaldi S, Hajjam ME, Mesurille B. Pulmonary embolism detection: Prospective evaluation of dual-section helical CT versus selective pulmonary arteriography in 157 patients. Radiology 2000;217:447–455. [PubMed: 11058644]

14. Goodman L, Curtin J, Mewissen M. Detection of pulmonary embolism in patients with unsolved clinical and scintigraphic diagnosis: Helical CT versus angiography. AJR Am J Roentgenol 1995;164:1369–1374. [PubMed: 7754875]

15. Senac J, Verhnet H, Bousquet C. Embolie pulmonaire: Apport de la tomodensitometrie helicoidale. J Radiol 1995;76:339–345. [PubMed: 7473363]

16. Rossum, Av; Pattynama, P.; Ton, E. Pulmonary embolism: Validation of spiral CT angiography in 149 patients. Radiology 1996;201:467–470. [PubMed: 8888242]

17. Remy-Jardin M, Remy J, Petyt L, Duhamel A. Diagnosis of acute pulmonary embolism with spiral CT: Comparison with pulmonary angiography and scintigraphy. Radiology 1996;200:699–706. [PubMed: 8756918]

18. Ferretti G, Bosson J, Buffaz P. Acute pulmonary embolism: role of helical CT in 164 patients with intermediate probability at ventilation-perfusion scintigraphy and normal results at duplex US of the legs. Radiology 1997;205:453–458. [PubMed: 9356628]

19. Rossum AV, Pattynama P, Mallens W, Herman J. Can helical CT replace scintigraphy in the diagnostic process in suspected pulmonary embolism? A retrolective-prolective cohort study focusing on total diagnostic yield. Eur Radiol 1998;8:90–96. [PubMed: 9442137]

20. Drucker E, Rivitz S, Shepard J. Acute pulmonary embolism: Assessment of helical CT for diagnosis. Radiology 1998;209:235–241. [PubMed: 9769837]

21. Herold C, Remy-Jardin M, Grenier P. Prospective evaluation of pulmonary embolism: initial results of the European multicenter trial (ESTIPEP). Radiology 1998;209:299.abstract

22. Garg K, Welsh C, Feyerabend A. Pulmonary embolism: Diagnosis with spiral CT and ventilation-perfusion scanning-correlation with pulmonary angiographic results or clinical outcome. Radiology 1998;208:201–208. [PubMed: 9646814]

23. Baghaie F, Remy-Jardin M, Remy J, Fribourg M. Diagnosis of peripheral acute pulmonary emboli: Optimization of the spiral CT acquisition protocol. Radiology 1998;209:299.abstract

24. Kim K, Muller N, Mayo J. Clinically suspected pulmonary embolism: Utility of spiral CT. Radiology 1999;210:693–697. [PubMed: 10207469]

25. Masutani Y, MacMahon H, Doi K. Computerized detection of pulmonary embolism in spiral CT angiography based on volumetric image analysis. IEEE Trans Med Imaging 2002;21:1517–1523. [PubMed: 12588035]

26. Schoepf UO, Das M, Schneider AC, et al. Computer-aided detection (CAD) of segmental and subsegmental pulmonary embolism on 1-mm multidetector-row CT (MDCT) studies. Radiology 2002;225:384.abstract

27. Zhou, C.; Hadjiiski, LM.; Patel, S., et al. Computerized detection of pulmonary embolism in 3D computed tomographic (CT) images. Presented at RSNA 2003; Chicago. November 30–December 5, 2003; p. 51

28. Zhou C, Hadjiiski LM, Sahiner B, et al. Computerized detection of pulmonary embolism in 3D computed tomographic (CT) images: Vessel tracking and segmentation techniques. Proc SPIE 2003;5032:1613–1620.

29. Higgins WE, Spyra WJT, Warwoski RA, Ritman EL. System for analyzing high-resolution three dimensional coronary angiograms. IEEE Trans Med Imaging 1996;15:377–385. [PubMed: 18215918]

30. Dempster AP, Laird NM, Rubin DB. Maximum likelihood from incomplete data via the EM algorithm. J R Stat Soc 1977;39:1–38.

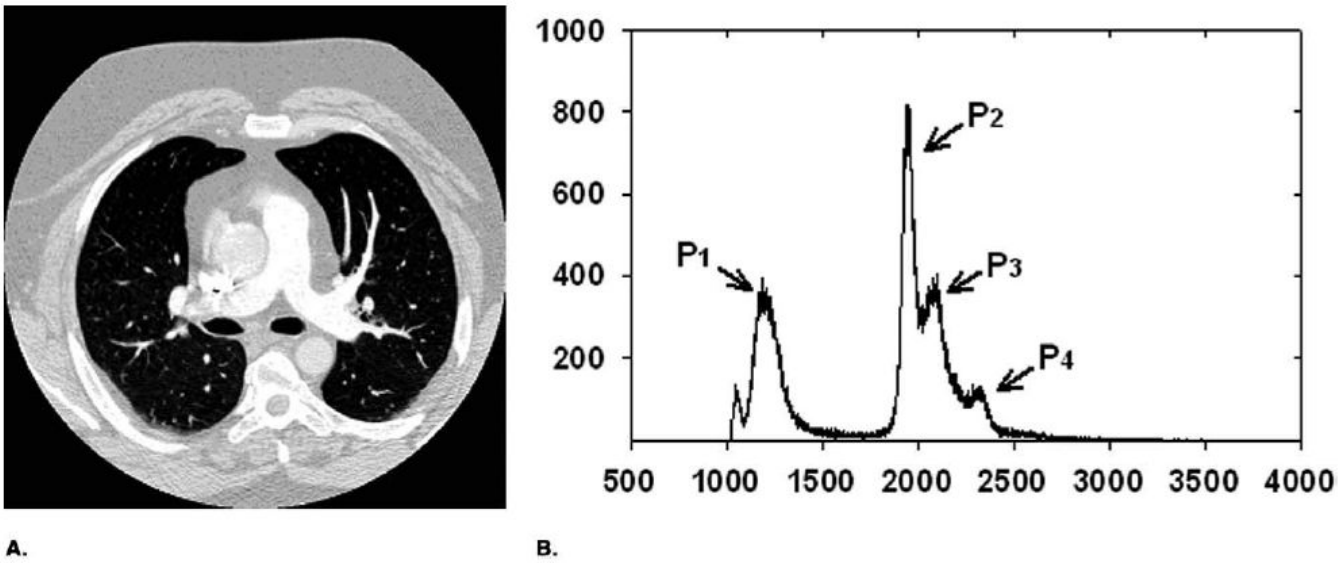

Figure 1.
(a) Typical CT slice image after DC component shifting. **(b)** Histogram of thoracic region excluding zero gray level. P_1, lung air region; P_2, P_3, chest wall and soft tissue, and P_4, vessel and heart.

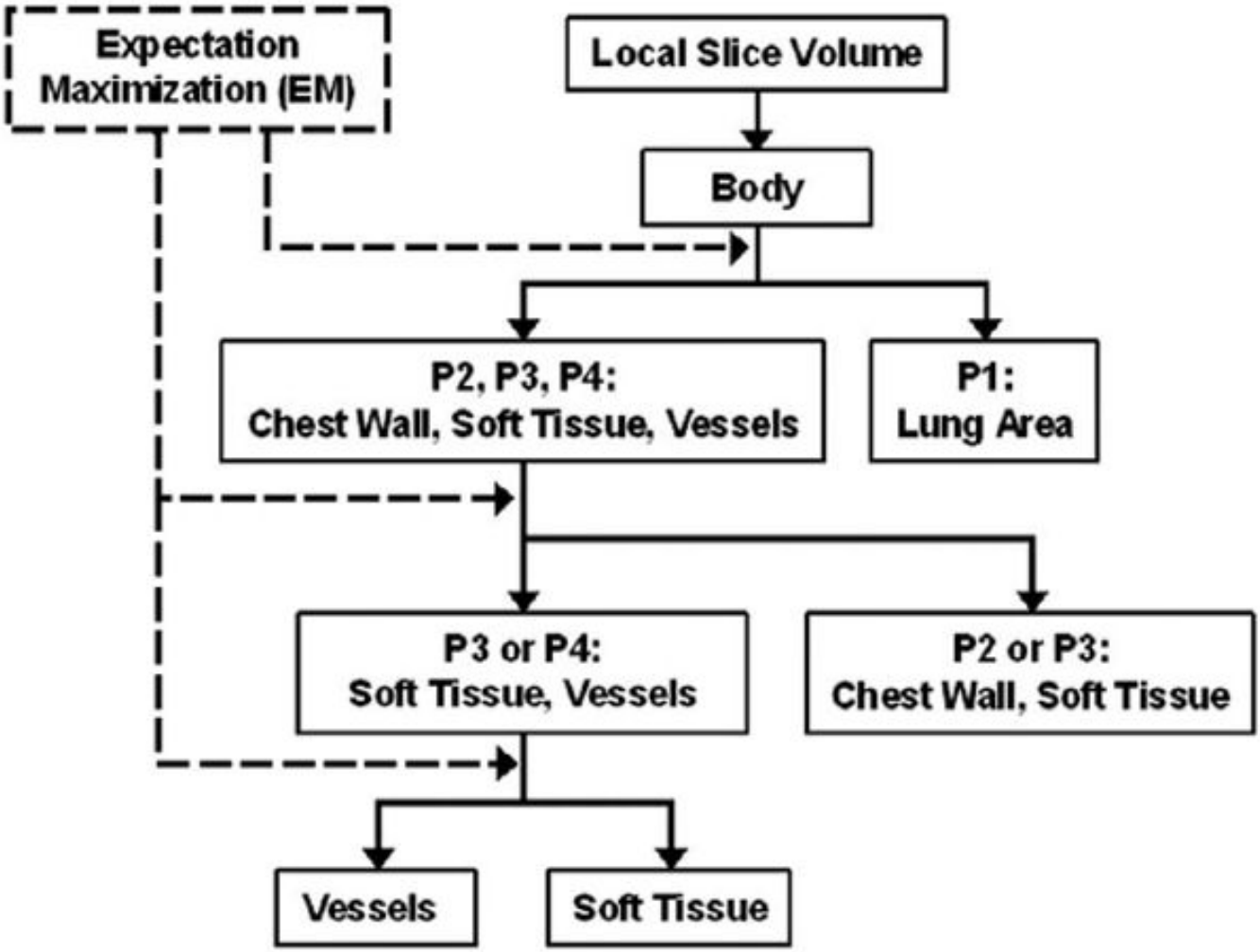

Figure 2.
Vessel segmentation scheme using EM algorithm.

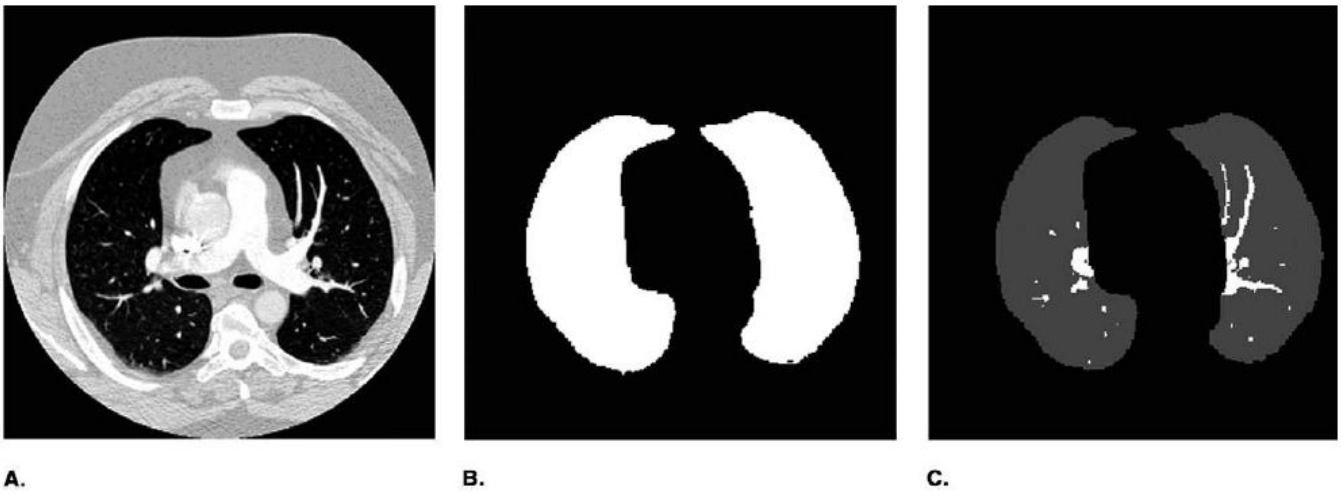

Figure 3.
An example of vessel segmentation. **(a)** Original image. **(b)** Lung region. **(c)** Segmented pulmonary arteries in lung region.

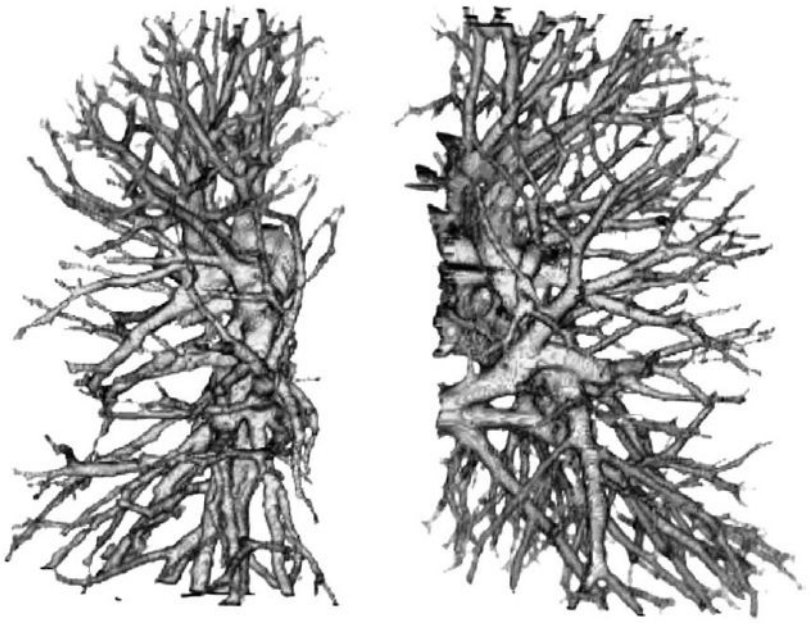

Figure 4.
An example of a tracked pulmonary vessel tree.

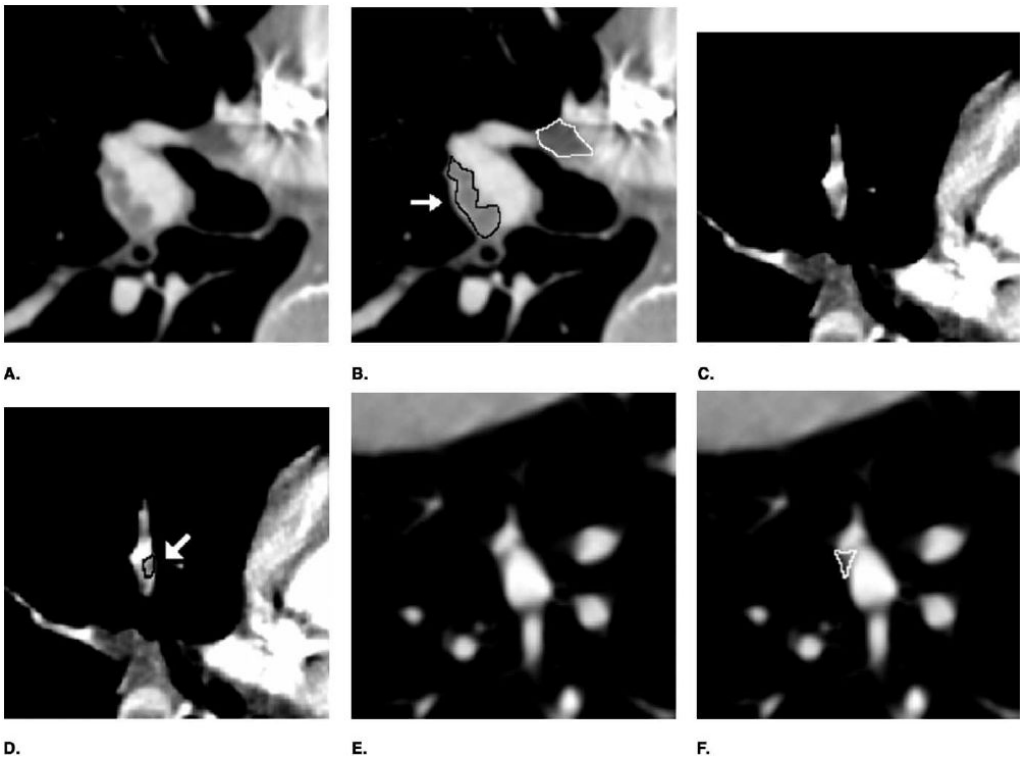

Figure 5.
Example of the computer detection. **(a, c, e)** Original image. **(b, d, f)** Detection result. A true-positive PE was enclosed by a black contour and marked by an *arrow*, a false-positive PE was enclosed by a white contour.

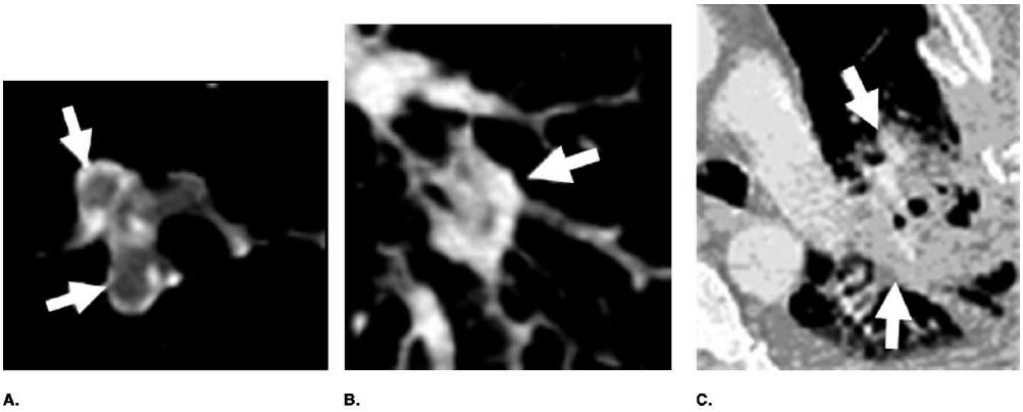

Figure 6.
Examples of difficult cases for vessel segmentation and tracking. **(a)** Artery was occluded by PEs (*arrows*). **(b, c)** Artery was surrounded by lung disease.

Table 1

Computer Performance If the Conspicuity of PE >2 (Ratings from 1 to 5, 5 Being the Most Conspicuous) and the PE Partially (20–80%) Occluded an Artery

Cases		All Arteries	Proximal	Subsegmental	False-Positives per Case
All Cases (14 cases)	Truth (n)	51	37	14	14.4
	True-positive (n)	40	31	9	
	Sensitivity (%)	78.4	83.8	64.3	
Without lung diseases (6 cases)	Truth (n)	34	25	9	18.3
	True-positive (n)	30	23	7	
	Sensitivity (%)	88.2	92.0	77.8	
With lung diseases (8 cases)	Truth (n)	17	12	5	11.4
	True-positive (n)	10	8	2	
	Sensitivity (%)	58.8	66.7	40.0	

Table 2

Computer Performance When the Percentage of the PE Occlusion in a Vessel Was ≤20% or ≥80% and the PE Conspicuity Was >2

Cases		Conspicuity >2 and PE% ≤20%		Conspicuity >2 and PE% ≥80%	
		Proximal	Subsegmental	Proximal	Subsegmental
All cases (14 cases)	Truth (n)	23	9	27	30
	True-positive (n)	15	3	16	8
	Sensitivity (%)	65.2	33.3	59.3	26.7
Without lung diseases (6 cases)	Truth (n)	12	6	15	16
	True-positive (n)	8	2	11	6
	Sensitivity (%)	66.7	33.3	73.3	37.5
With lung diseases (8 cases)	Truth (n)	11	3	12	14
	True-positive (n)	7	1	5	2
	Sensitivity (%)	63.6	33.3	41.7	14.3

Table 3

Computer Performance if the PE Occluded an Artery in the Ranges of 20%–80%, ≤20%, and ≥80% at Any Conspicuity Level (1-5)

Cases		PE 20%–80%		PE% ≤20%		PE% ≥80%		All	
		Proximal	Subsegmental	Proximal	Subsegmental	Proximal	Subsegmental	Proximal	Subsegmental
All cases (14 cases)	Truth (n)	40	17	26	13	28	39	94	69
	True-positive (n)	31	10	16	3	16	9	63	22
	Sensitivity (%)	77.5	58.8	61.5	23.1	57.1	23.1	67.0	31.9
Without lung diseases (6 cases)	Truth (n)	26	11	15	8	16	25	57	44
	True-positive (n)	23	8	9	2	11	7	43	17
	Sensitivity (%)	88.5	72.7	60.0	25.0	68.8	28.0	75.4	38.6
With lung diseases (8 cases)	Truth (n)	14	6	11	5	12	14	37	25
	True-positive (n)	8	2	7	1	5	2	20	5
	Sensitivity (%)	57.1	33.3	63.6	20.0	41.7	14.3	54.1	20